

## Article

# Guest Molecules with Amino and Sulfhydryl Groups Enhance Photoluminescence by Reducing the Intermolecular Ligand-to-Metal Charge Transfer Process of Metal–Organic Frameworks

Yuewu Zhao <sup>1</sup>, Jine Wang <sup>1,2,\*</sup> and Renjun Pei <sup>1,2,\*</sup>

<sup>1</sup> CAS Key Laboratory of Nano-Bio Interface, Suzhou Institute of Nano-Tech and Nano-Bionics, Chinese Academy of Sciences, Suzhou 215123, China

<sup>2</sup> School of Nano Technology and Nano Bionics, University of Science and Technology of China, Hefei 230026, China

\* Correspondence: jewang2012@sinano.ac.cn (J.W.); rjpei2011@sinano.ac.cn (R.P.)

**Abstract:** Micron-sized metal–organic framework (MOF) sheets were prepared using organic molecules with aggregation-induced emission (AIE) properties as ligands. The intermolecular ligand-to-metal charge transfer (LMCT) process occurs in MOF structures, resulting in the disappearance of the matrix coordination-induced emission (MCIE) effect and emergence of the aggregation-caused quenching (ACQ) effect. Here, we demonstrate that molecules with electron donors can compete with the LMCT process in MOF structures, thereby changing the transfer path of the excitation energy and returning it to the ground state, mainly in the form of fluorescence. Organic molecules with amino or sulfhydryl groups can act as effective electron donors, reducing the LMCT process and causing the MCIE effect of the MOF sheet. The coexistence of amino and sulfhydryl groups will strongly inhibit the LMCT process of the MOF sheet, thereby greatly enhancing the MCIE effect. Therefore, these types of molecules can be used to regulate the photoluminescence intensity of AIE-based MOF materials. In addition, there are some organic molecules with multiple carboxyl or hydroxyl groups which can produce similar effects. Finally, it was confirmed that the intermolecular LMCT process is highly sensitive, and the MOF sheet showed distinguishable fluorescence results even with the addition of small molecules in the amount of  $10^{-9}$  M. Thus, it is a feasible idea to use the fluorescence changes induced by the LMCT process as a sensitive sensing method for small molecules.

**Keywords:** metal–organic framework; aggregation-induced emission; ligand-to-metal charge transfer; matrix coordination-induced emission; sensitive



**Citation:** Zhao, Y.; Wang, J.; Pei, R. Guest Molecules with Amino and Sulfhydryl Groups Enhance Photoluminescence by Reducing the Intermolecular Ligand-to-Metal Charge Transfer Process of Metal–Organic Frameworks. *Appl. Sci.* **2022**, *12*, 11467. <https://doi.org/10.3390/app122211467>

Academic Editor: Vardan Galstyan

Received: 14 October 2022

Accepted: 10 November 2022

Published: 11 November 2022

**Publisher's Note:** MDPI stays neutral with regard to jurisdictional claims in published maps and institutional affiliations.



**Copyright:** © 2022 by the authors. Licensee MDPI, Basel, Switzerland. This article is an open access article distributed under the terms and conditions of the Creative Commons Attribution (CC BY) license (<https://creativecommons.org/licenses/by/4.0/>).

## 1. Introduction

A metal–organic framework (MOF) is an ordered porous structure obtained using the coordination of organic ligands with metal ions or metal clusters [1–3]. The large surface area, multiple active sites, high porosity, and structural flexibility enable MOF materials to exhibit excellent performance in multiple fields, such as catalysts [4], sensors [5–7], bioimaging [8,9], tumor therapy [10–12], gas storage or separation [13,14], and solar fuel conversion [15,16]. Yaghi et al. demonstrated that MOF materials can be used effectively for methane storage with a storage capacity of 240 cubic centimeters [17], and then they developed MOF structural materials for highly efficient hydrogen storage [18]. Long et al. conducted in-depth research on the interaction mechanism between MOF materials and carbon dioxide, and expounded the application prospects of MOF materials for carbon dioxide adsorption, capture, and separation [19–21]. MOF materials also have unique application advantages in drug delivery [22,23], and even more MOF nanomaterials have been developed for photodynamic, photothermal, and other treatments of tumors [24–27]. MOF materials have accessible active sites based on the monodispersity of the constituent

molecules in their coordination structure, which can be used as sensors for highly sensitive detection of small molecules and environmental pollutants [28–30]. Therefore, the construction of organic molecules into MOF structural materials through a certain coordination method has great potential to perform well in various applications.

Molecules with a propeller-like structure make up a family of compounds with an aggregation-induced emission (AIE) effect discovered by Tang et al. [31]. Such molecules can restrict the intramolecular rotation through aggregation, and release energy in the form of photoluminescence, thus exhibiting the AIE phenomenon. Compared with the traditional aggregation-caused quenching (ACQ) effect molecules, AIE molecules have unique advantages in optoelectronics, sensing, and biomedical applications [32,33]. The MOF structure is essentially an aggregation of molecules, and this matrix coordination-induced emission (MCIE) effect has also been verified using MOF materials constructed with tetraphenylethylene (TPE) molecules and zinc ions [34]. Zhou et al. demonstrated the MCIE effect of AIE molecules using zirconium-based MOF materials, and analyzed their quantum yield and piezofluorochromic properties [35,36]. However, not all MOF materials constructed from AIE molecules have the MCIE effect, and it has been found that changing the types of metal ions in the MOF structure influences its photoluminescence intensity. When Co and Cu ions are used as metal-coordination ions in the MOF, even the material constructed using AIE molecules exhibits the ACQ phenomenon [37,38]. This result was verified by means of comparative analysis in our previous work, and the intermolecular ligand-to-metal charge transfer (LMCT) process in the MOF structure was described as the main reason for the ACQ phenomenon [39]. In addition, we found that the guest molecules can affect the photoluminescence of the MOF host. Of course, there are other studies on the applications of host–guest molecules [40–42].

In this paper, we designed and synthesized a micron-sized MOF sheet with AIE molecules as organic ligands, and identified that organic molecules with amino or sulfhydryl groups can reduce the LMCT process in MOF structures. The organic molecules with both amino and sulfhydryl groups can greatly hinder the LMCT process, resulting in a strong MCIE effect on the MOF sheet originally with the ACQ results. Moreover, the fluorescence generated using this LMCT process can produce a sensitive sensing effect on molecules, even up to  $10^{-9}$  M. These studies have theoretical guiding significance for regulating the energy release mode and photoluminescence intensity of MOF materials. Based on the intermolecular LMCT process, a nanoscale ultra-sensitive detection method has been proposed.

## 2. Experimental Section

### 2.1. Materials

4,4,4-(Ethane-1,1,2,2-tetrayl)tetrabiphenyl-4-carboxylic acid (97%, H<sub>4</sub>ETTC) was purchased from Shanghai Tensus Biotech Co., Ltd. (China). Copper(II) nitrate hydrate, L-tryptophan, and citric acid were obtained from Sinopharm Chemical Reagent Co., Ltd. (Shanghai, China). Lipoic acid was obtained from Energy Chemical Co., Ltd. (Shanghai, China). 3,3'-dithiodipropionic acid, glycine, L(+)-arginine, L-aspartic acid, DL-dithiothreitol, and L(+)-ascorbic acid were purchased from Sigma-Aldrich Chemical Co., Ltd. (Shanghai, China). 2,2'-dithiodiethanol, 3-mercaptopropionic acid, N-acetyl-L-cysteine, and glutathione were obtained from TCI Development Co., Ltd. (Shanghai, China). DL-homocystine was purchased from Aladdin Chemical Co., Ltd. (Shanghai, China). L-lysine was obtained from Sangon Biotech Co., Ltd. (Shanghai, China). L-kynurenine and succimer were purchased from Shanghai Titan Technology Co., Ltd. (China). All other chemicals were analytical grade and used without further purification. Deionized water was prepared with a Milli-Q purification system.

### 2.2. Synthesis of Cu-ETTC MOF Sheet

In a typical procedure of Cu-ETTC MOF sheet preparation, an aqueous solution of 10 mM copper nitrate (4 mL or 2 mL) was mixed with a DMF solution of 10 mM H<sub>4</sub>ETTC (2 mL), and then 20 mL of DMF solution was added and mixed evenly. Subsequently, the

mixture was reacted at 90 °C for 1 h under stirring conditions, and the blue Cu-ETTC MOF product was obtained. The obtained solution containing MOF products was centrifuged, and then washed twice with ethanol to remove unreacted organic matter and residual copper ions. Finally, it was washed with deionized water to obtain pure Cu-ETTC products.

### 2.3. Effect of Different Molecules on Fluorescence of MOF Sheet

The Cu-ETTC MOF sheet was mixed with lipoic acid, 3,3'-dithiodipropionic acid, 2,2'-dithiodiethanol, DL-homocystine, glycine, L-lysine, L(+)-arginine, L-aspartic acid, L-tryptophan, L-kynurenine, DL-dithiothreitol, 3-mercaptopropionic acid, succimer, N-acetyl-L-cysteine, glutathione, citric acid, and L(+)-ascorbic acid, and reacted in the dark for 2 h. Finally, the fluorescence intensity was measured at the instrument voltage of 375 V. The concentrations of the MOF and these molecules in the reaction solution were both 50 µM. The concentration of the MOF was based on the content of Cu element in its structure, which was determined using inductively coupled plasma mass spectrometry (ICP-MS). An excitation wavelength of 360 nm and a slit of 10 nm were used in all fluorescence experiments.

### 2.4. Effect of Different MOF Contents on Fluorescence in Glutathione Solution

Different concentrations of the Cu-ETTC MOF sheet were mixed with glutathione, reacted in the dark for 2 h, and the resulting fluorescence intensity was measured at 375 V. The concentration of glutathione and MOF in the reaction solution were 125 µM and 0, 1.56, 3.13, 6.25, 12.5, 25, and 50 µM, respectively. Finally, the fluorescence of the MOF concentration in 3.13 µM was measured by changing the voltage of the instrument.

### 2.5. Effect of Different Amounts of Glutathione on Fluorescence of MOF Sheet

Different concentrations of glutathione were mixed with the Cu-ETTC MOF sheet, reacted in the dark for 2 h, and the resulting fluorescence intensity was measured at 950 V. The concentrations of MOF and glutathione in the reaction solution were 5 nM (or 50 nM) and 0, 2, 4, 6, 8, and 10 nM (or 0, 20, 40, 60, 80, and 100 nM), respectively.

### 2.6. Characterizations

The morphology of the Cu-ETTC MOF was characterized using a Hitachi HT7700 transmission electron microscope (TEM). The absorption spectra were analyzed using a Shimadzu 1280 UV-visible spectrophotometer. Fourier transform infrared spectroscopy (FT-IR) was characterized using a Thermo Scientific Nicolet iS20 spectrometer. X-ray photoelectron spectroscopy (XPS) tests were performed using a Thermo Scientific K-Alpha+ instrument. The fluorescence intensity was analyzed using a Hitachi F4600 fluorescence photometer.

## 3. Results and Discussion

As shown in Figure 1a, the Cu-ETTC MOF sheet was synthesized by reacting 4,4,4,4-(ethene-1,1,2,2-tetra-yl)tetrabiphenyl-4-carboxylic acid and copper(II) nitrate hydrate in N,N-dimethylformamide (DMF) solvent using the bottom-up method. Based on the limitations of intramolecular rotation, in theory, H<sub>4</sub>ETTC will release excitation energy mainly in the form of AIE effect after forming the MOF structure. However, the Cu-ETTC MOF sheet also suffers from the intermolecular LMCT process, resulting in the opposite phenomenon and an aggregation-caused quenching effect. Figure 1b shows the photograph images obtained under natural light and 365 nm wavelength conditions, where the fluorescence of Cu-ETTC is almost completely quenched. Then, the chemical structure and morphology of the Cu-ETTC MOF sheet were analyzed using a UV-vis absorption spectra, Fourier transform infrared spectroscopy (FT-IR), X-ray photoelectron spectroscopy (XPS), and transmission electron microscopy (TEM). As shown in Figure 1c, the H<sub>4</sub>ETTC exhibited a broad absorption profile with three discernible feature peaks at 291, 318, and 362 nm. With the formation of the Cu-ETTC MOF sheet, a significant absorption peak appeared at 272 nm, and the position of the strongest absorption peak changed from 291 to 324 nm,



The prepared Cu-ETTC MOF has an obvious two-dimensional ultrathin-layered morphology with a graphene-like multi-wrinkled structure, linked at a micron size. As shown in Figure 2a, after reducing the proportion of coordinated metals, the MOF material still had a lamellar structure, but the wrinkles were significantly reduced, showing a separate lamellar morphological distribution with different particle sizes. Therefore, a more homogeneous MOF material was selected for research in this study, that is, the sample obtained as the  $\text{Cu}(\text{NO}_3)_2/\text{H}_4\text{ETTC}$  reaction ratio was 2/1. To elucidate the elemental information of the Cu-ETTC MOF sheet, XPS analysis was carried out. The C, O, and Cu elements appeared in the XPS spectrum of the Cu-ETTC MOF sheet, and their contents were 84.36, 13.9, and 1.74%, respectively. As shown in Figure 2d, the binding energy (BE) peaks at 935.0 and 954.9 eV were assigned to  $\text{Cu}^{2+}$ , accompanied by the characteristic shakeup satellite peaks at 940.2, 944.2, 960.1, and 963.2 eV. The BE peaks of Cu  $2p_{3/2}$  and Cu  $2p_{1/2}$  at 933.4 and 953.2 eV, respectively, confirmed the presence of a large amount of  $\text{Cu}^+$  in the Cu-ETTC MOF structure. This result also demonstrated that the Cu-ETTC MOF sheet has a significant LMCT process, and this process annihilates the matrix coordination-induced emission (MCIE) effect. In addition, the Cu-O BE at 533 eV in Figure 2c further confirms the coordination chelation of metallic copper with the porphyrin carboxyl group. On the basis of the aforementioned results, the two-dimensional Cu-ETTC MOF sheet was formed using coordination chelation between  $\text{H}_4\text{ETTC}$  and  $\text{Cu}(\text{II})$  paddlewheel ( $\text{Cu}_2(\text{COO})_4$ , secondary structure units) metal nodes [43].

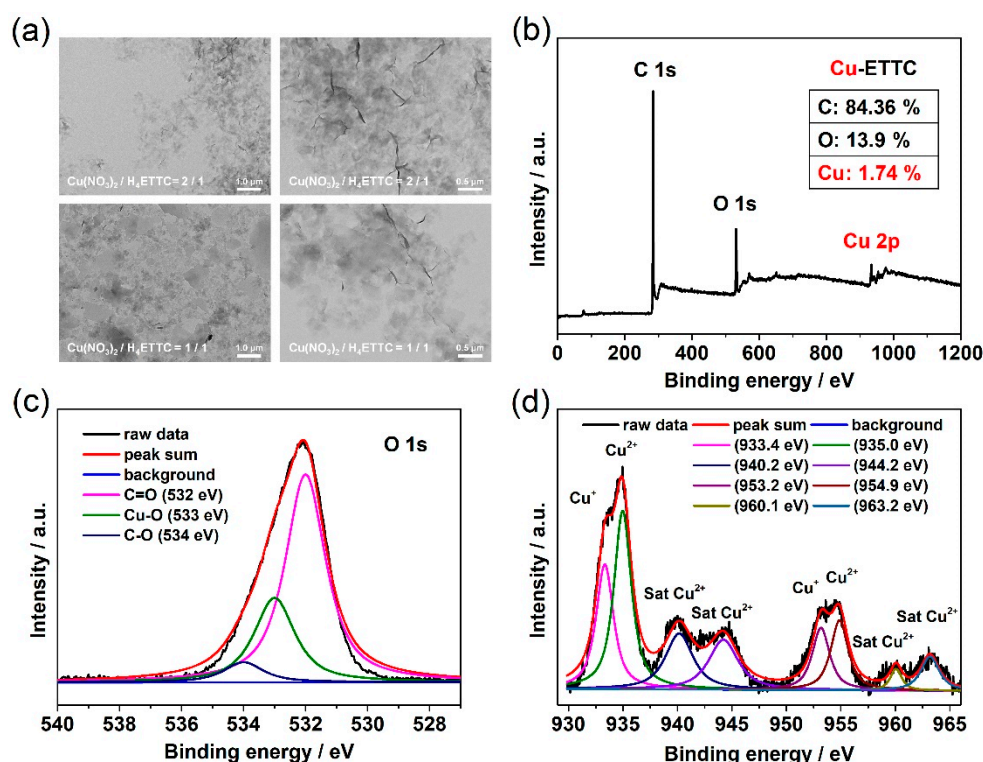


**Figure 2.** (a) TEM images of the Cu-ETTC MOF sheet obtained at different reaction molar ratios. (b) Full XPS, (c) O 1s, and (d) Cu 2p spectrum of the Cu-ETTC MOF sheet.

Since the MOF sheet constructed using  $\text{H}_4\text{ETTC}$  and copper ions causes the ACQ effect, the question of which molecules can restore the fluorescence of Cu-ETTC materials has become worth exploring. As shown in Figure 3a, an energy-level transition occurs after the MOF sheet is excited from the  $S_0$  ground state to the high-energy  $S_n$  excited state. Subsequently, the  $S_n$  excitation energy will reach the  $S_1$  excited state through vibrational relaxation and internal transitions, and finally return to the  $S_0$  ground state by releasing the excitation energy in the form of fluorescence and nonradiative energy. However, there is an LMCT process in the Cu-ETTC MOF structure, which transfers the  $S_1$  excitation energy

to the metal nodes, resulting in apparent fluorescence quenching. If an electron donor is added to compete with the LMCT process to produce a reduced or blocked effect, the  $S_1$  excitation energy of the MOF sheet will still be released in the form of fluorescence, and the matrix coordination-induced emission effect will reappear (Figure 3b).

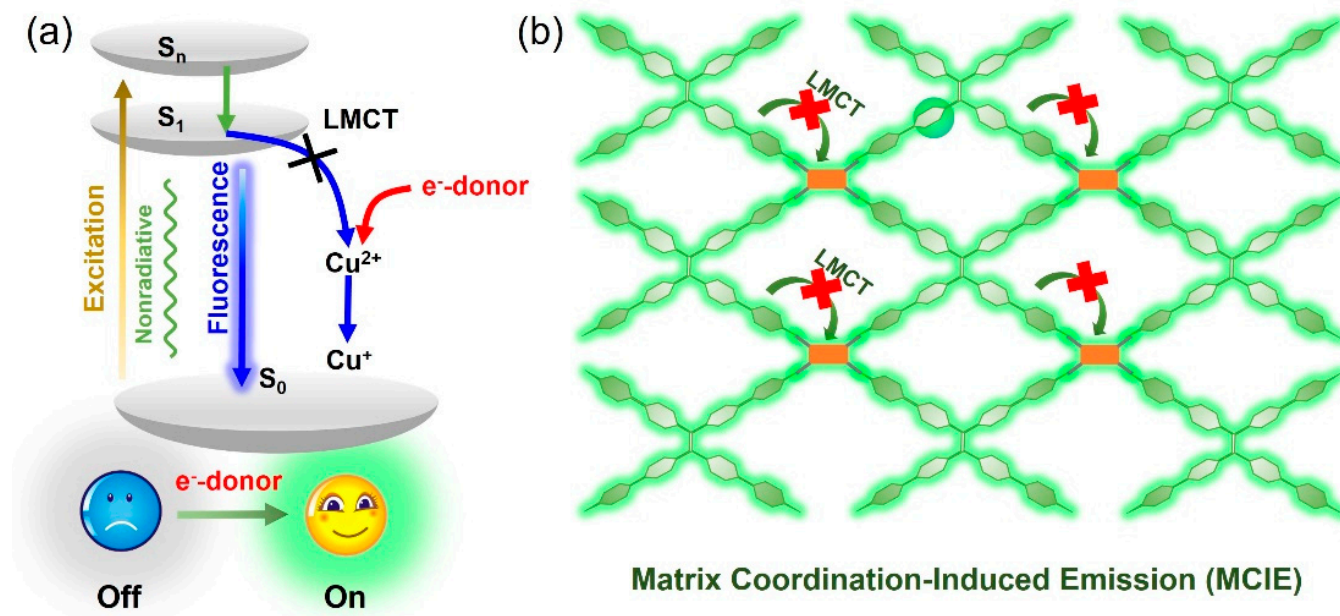


**Figure 3.** Schematic representation of (a) the excited energy transfer process and (b) the matrix coordination-induced emission effect.

In order to verify the hypothesis that electron donors can restore the fluorescence of the Cu-ETTC MOF sheet, we performed fluorescence recovery experiments using lipoic acid, 3,3'-dithiodipropionic acid, 2,2'-dithiodiethanol, DL-homocystine, glycine, L-lysine, L(+)-arginine, L-aspartic acid, L-tryptophan, L-kynurenine, DL-dithiothreitol, 3-mercaptopropionic acid, succimer, N-acetyl-L-cysteine, and glutathione. As shown in Figure 4a, the addition of lipoic acid, 3,3'-dithiodipropionic acid, and 2,2'-dithiodiethanol failed to awaken the fluorescence of the Cu-ETTC MOF sheet. However, DL-homocystine with a similar structure makes the MOF sheet emit strong fluorescence, with the obvious difference being that this molecular structure contains two amino groups. As a strong electron-donating group, the amino group can provide electrons to the copper metal nodes in the Cu-ETTC structure, reduce the intermolecular LMCT process in the MOF sheet, and make part of the  $S_1$  excitation energy express in the form of fluorescence. Therefore, it is logical that glycine can also cause the fluorescence recovery of the Cu-ETTC MOF sheet, but its fluorescence intensity is lower than that of DL-homocystine, which is due to the lower number of amino-donor groups. Subsequently, other types of amino acids were also analyzed. As shown in Figure 4b, these amino acids with different groups can give the MOF sheet a fluorescence recovery effect to a certain extent. The difference is only the degree of intensity, which mainly depends on whether the group attached contains electron donors or acceptors. In addition, some molecules containing sulfhydryl groups have been studied. As shown in Figure 4c, these sulfhydryl-containing molecules are all able to restore the fluorescence of the Cu-ETTC MOF sheet and have a strong effect, indicating that more  $S_1$  excitation energy is converted into fluorescence. Notably, two molecules, N-acetyl-L-cysteine and glutathione, which contain both amino and sulfhydryl groups, have strong effects in awakening the fluorescence of the Cu-ETTC MOF sheet.

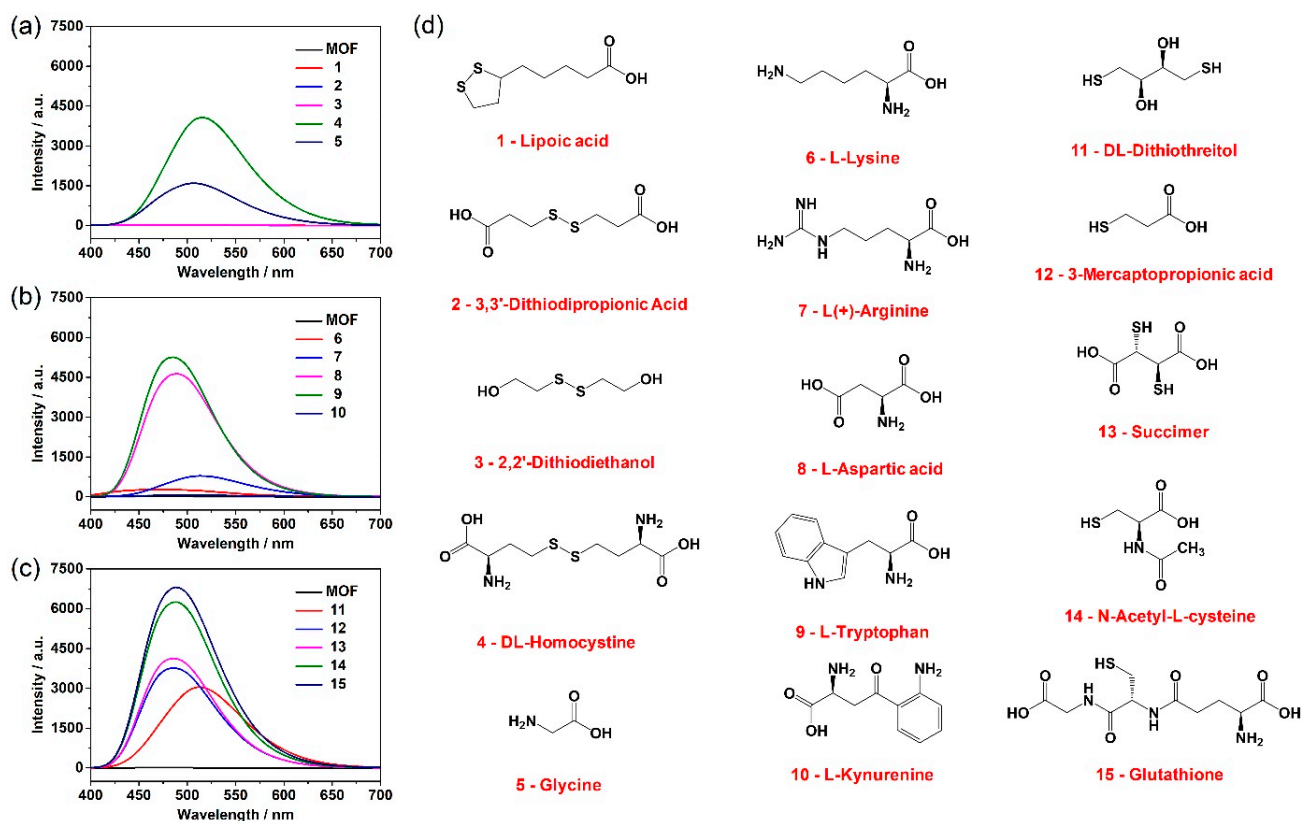


**Figure 4.** (a–c) Fluorescence intensity curves obtained by interaction of different molecules with the Cu-ETTC MOF sheet. The concentrations of the Cu-ETTC MOF sheet and other molecules were both 50  $\mu\text{mol/L}$ . (d) Serial number and corresponding molecular structure.

The influence of the above-mentioned molecules on the Cu-ETTC MOF sheet was then analyzed using a more intuitive histogram and peak-axis location distribution diagram. As shown in Figure 5a, molecules 1–3 mainly contain carboxyl and hydroxyl groups, which cannot effectively awaken the fluorescence of the MOF sheet. Molecules 4–10 are various amino acids, which can restore the fluorescence of the MOF sheet, but the different groups attached have a great influence on the fluorescence intensity. Molecules 11–13 are molecules with sulfhydryl groups, which can also effectively awaken the fluorescence of the MOF sheet. The coexistence of amino (imine) and sulfhydryl groups in molecules 14–15 can arouse the fluorescence of the MOF sheet strongly. Therefore, it may be a more effective method to reduce the intermolecular LMCT process in the MOF structure by using molecules with coexisting amino and sulfhydryl groups as electron donors. These results have certain guiding significance for adjusting the conversion route of  $S_1$  excitation energy and enhancing the fluorescence intensity of MOF materials. Interestingly, the peak-axis location of the Cu-ETTC MOF sheet also conforms to certain statistical laws. As shown in Figure 5b, the peak positions of the above-mentioned molecules are mainly distributed around 470, 490, and 510 nm, with a difference of about 20 nm, and the peak distribution positions are basically independent of the peak intensity.

In addition to the amino and sulfhydryl groups that can restore the fluorescence of the MOF sheet, some molecules with multiple carboxyl groups and multiple hydroxyl groups can also effectively reduce the intermolecular LMCT process in the Cu-ETTC structure and turn on the MOF sheet fluorescence switch. As shown in Figure 5c,d, citric acid and L(+)-ascorbic acid can arouse the fluorescence of the Cu-ETTC MOF sheet, although the specific electron-donating mechanism is still unclear. It is worth mentioning that the peak axes of citric acid and L(+)-ascorbic acid are located at 488 and 510 nm, respectively, which are still within the above distribution range.

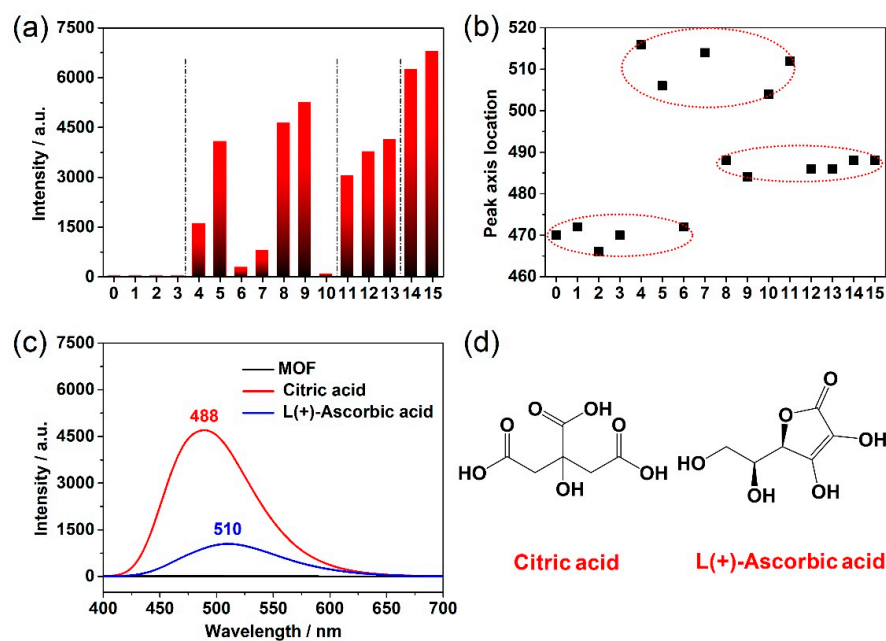


**Figure 5.** (a) Histogram of fluorescence intensity and (b) peak-axis location distribution generated using the reaction of a variety of the above molecules with the MOF sheet. (c) Fluorescence intensity curves obtained by interaction of citric acid and L(+)-ascorbic acid with the MOF sheet. (d) Corresponding molecular structure.

Compared with other molecules, glutathione has a stronger fluorescence-awakening effect on the Cu-ETTC MOF sheet. Therefore, the prepared a Cu-ETTC sheet with a large specific surface area may be viable for the sensitive detection of glutathione, because such MOF sheets have more active sites for copper. Glutathione mainly uses its electron-donating ability to arouse the fluorescence of the MOF sheet, so whether the amount of glutathione is sufficient becomes a major factor affecting the fluorescence intensity of the Cu-ETTC sheet. As shown in Figure 6b, under the condition of sufficient glutathione, the fluorescence intensity of the MOF enhanced with it showed a linear relationship at the concentration of about 0~25  $\mu\text{mol/L}$ . When continuing to increase the content of the MOF sheet, the increase in fluorescence decreased, thus showing a parabolic profile (Figure 6c), which may be due to the difficulty for glutathione to provide enough electrons to reduce the LMCT process in the Cu-ETTC MOF structure. Therefore, based on this mechanism of action between Cu-ETTC and glutathione, the MOF sheet can only have a linear relationship with glutathione within a certain matching range. In addition, the instrument voltage used in the test has a considerable influence on its sensitivity. As shown in Figure 6a, the fluorescence intensity of the Cu-ETTC MOF sheet showed a huge transition with the voltage of the instrument, and even increased by about 10 times. Therefore, the use of larger voltages is an effective way to increase the detection sensitivity.

Finally, the detection sensitivity of the Cu-ETTC MOF sheet for glutathione was analyzed using a larger instrument voltage. As shown in Figure 7, the MOF sheet has a high detection sensitivity for glutathione and still has an obvious linear relationship at the amount of  $10^{-9}$  M, where the relevant linear regression equations are  $y = 455.57 + 4.549x$  and  $y = 162.9 + 32.59x$ . Although the Cu-ETTC MOF sheet can detect glutathione sensitively, considering the matching relationship between glutathione and the MOF sheet, this detection method, which enhances fluorescence by reducing the intermolecular LMCT process, has certain limitations in the linear range of detection. In addition, the use of a high voltage and low concentration makes the Cu-ETTC MOF sheet generate a certain fluorescence signal-to-noise ratio, and the obtained signal has a large fluctuation. Overall, the utilization of electron donors to reduce the LMCT process in MOF structures is a feasible method and has high sensitivity in molecular detection applications. However,

many molecules have electron-donor effects, which makes the MOF less advantageous in terms of detection specificity. Every coin has two sides, but the Cu-ETTC MOF sheet has detection sensitivity for a variety of electron-donating molecules, which makes it suitable for a wide range of applications.

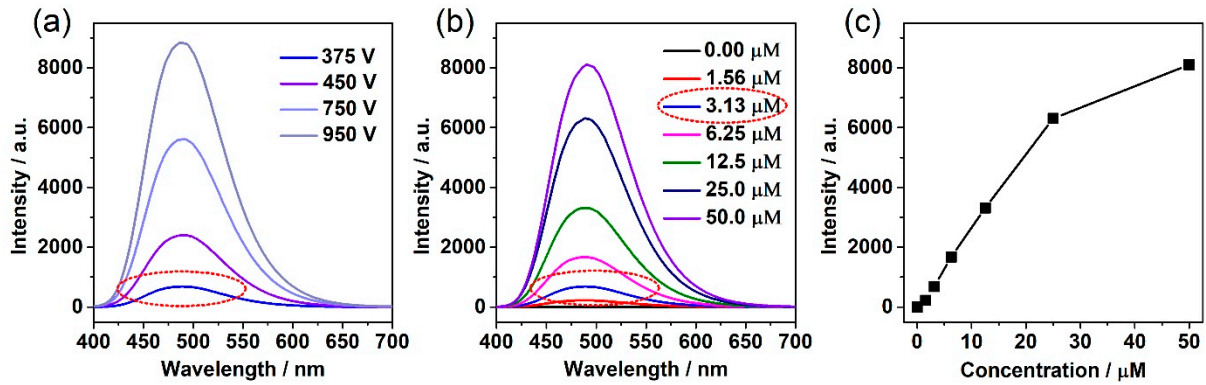


**Figure 6.** (a) Fluorescence intensity curves obtained by interaction of glutathione (125 μmol/L) with Cu-ETTC (3.13 μmol/L) under different voltage conditions of the instrument. (b) Fluorescence intensity curves obtained by interaction of glutathione (125 μmol/L) with different Cu-ETTC sheets at 375 V. (c) Correlation linearity of Cu-ETTC with different concentrations.

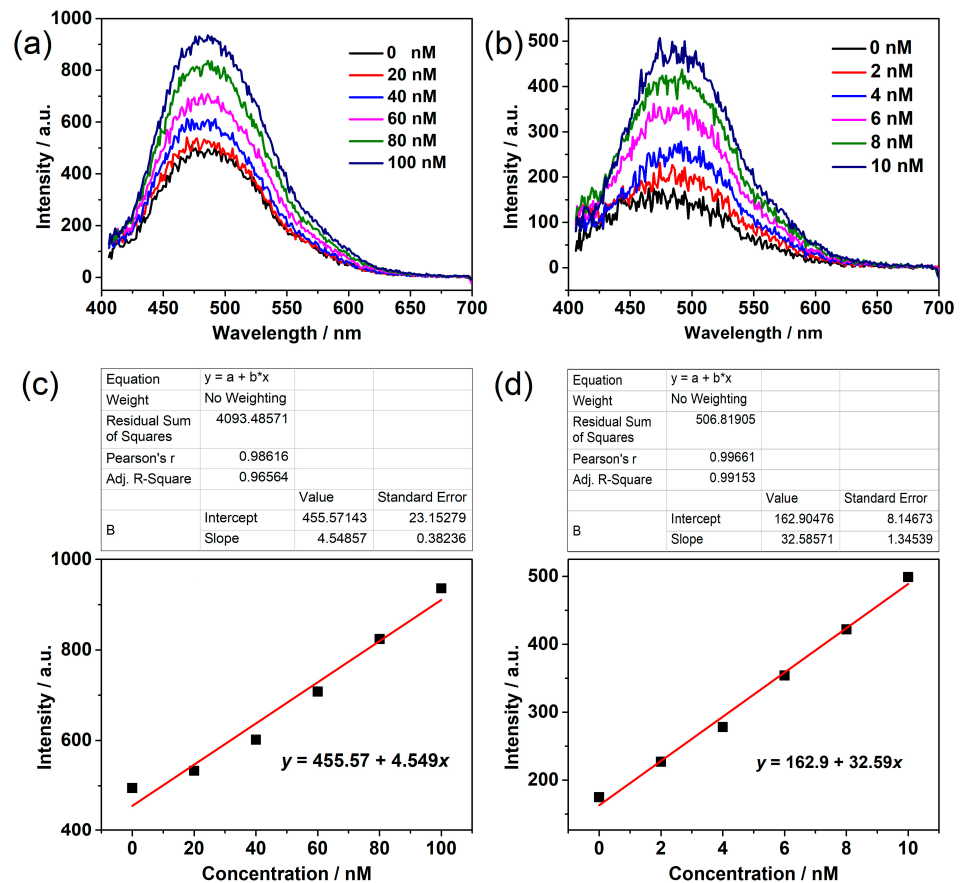


**Figure 7.** (a) Fluorescence intensity curves and (c) correlation linearity obtained by interaction of the Cu-ETTC MOF sheet (50 nmol/L) with different glutathione concentrations at 950 V. (b) Fluorescence intensity curves and (d) correlation linearity obtained by interaction of the Cu-ETTC MOF sheet (5 nmol/L) with different glutathione concentrations at 950 V.

#### 4. Conclusions

In summary, a micron-sized Cu-ETTC MOF sheet was constructed through the coordination binding reaction of H<sub>4</sub>ETTC molecules with copper ions. The intermolecular LMCT process within the MOF structure prevented the MCIE effect that AIE molecules should have exhibited, thereby creating the ACQ effect. Electron-donating molecules with amino and sulfhydryl groups can effectively reduce the LMCT process in the Cu-ETTC MOF structure. By regulating the excitation energy of the S<sub>1</sub> state, a greater amount of absorbed energy is released in the form of fluorescence, thus playing the role of awakening the MCIE effect of the MOF sheet. Moreover, molecules with both amino and sulfhydryl groups showed a better performance in arousing the fluorescence of the Cu-ETTC MOF sheet. It is worth mentioning that this method of manipulating S<sub>1</sub> excitation energy to release fluorescence using electron donor molecules has extremely high sensitivity, even up to the amount of 10<sup>-9</sup> M. This study provides some experimental results for selecting molecules with efficient electron-donating groups, and it illustrates possible theoretical directions for manipulating the excitation energy of the S<sub>1</sub> state.

**Author Contributions:** Conceptualization, R.P. and Y.Z.; methodology, J.W.; software, Y.Z.; data curation, R.P., J.W., and Y.Z.; writing—original draft preparation, Y.Z.; writing—review and editing, R.P. and J.W.; supervision, R.P.; funding acquisition, Y.Z. and J.W. All authors have read and agreed to the published version of the manuscript.

**Funding:** This research was funded by the National Natural Science Foundation of China, grant number 31900999 and 32071392. And the Natural Science Foundation of Jiangsu Province, grant number BE2020766 and BK20221264. And the China Postdoctoral Science Foundation, grant number 2021T140500. And the Jiangsu Planned Projects for Postdoctoral Research Funds, grant number 2021K070A. And the Basic Research Pilot Project in Suzhou, grant number SJC2022006. And the Science Foundation of Jiangxi Province, grant number 20192ACB21033.

**Institutional Review Board Statement:** Not applicable.

**Informed Consent Statement:** Not applicable.

**Data Availability Statement:** Not applicable.

**Conflicts of Interest:** The authors declare no competing financial interests.

#### References

1. James, S.L. Metal-organic frameworks. *Chem. Soc. Rev.* **2003**, *32*, 276–288. [[CrossRef](#)] [[PubMed](#)]
2. Furukawa, H.; Cordova, K.E.; O’Keeffe, M.; Yaghi, O.M. The chemistry and applications of metal-organic frameworks. *Science* **2013**, *341*, 1230444. [[CrossRef](#)] [[PubMed](#)]
3. Li, J.R.; Sculley, J.; Zhou, H.C. Metal-organic frameworks for separations. *Chem. Rev.* **2012**, *112*, 869–932. [[CrossRef](#)] [[PubMed](#)]
4. Kornienko, N.; Zhao, Y.; Kley, C.S.; Zhu, C.; Kim, D.; Lin, S.; Chang, C.J.; Yaghi, O.M.; Yang, P. Metal-organic frameworks for electrocatalytic reduction of carbon dioxide. *J. Am. Chem. Soc.* **2015**, *137*, 14129–14135. [[CrossRef](#)]
5. Hu, Z.; Deibert, B.J.; Li, J. Luminescent metal-organic frameworks for chemical sensing and explosive detection. *Chem. Soc. Rev.* **2014**, *43*, 5815–5840. [[CrossRef](#)]
6. Koo, W.T.; Jang, J.S.; Kim, I.D. Metal-organic frameworks for chemiresistive sensors. *Chem* **2019**, *5*, 1938–1963. [[CrossRef](#)]
7. Zhao, Y.; Jiang, L.; Shangguan, L.; Mi, L.; Liu, A.; Liu, S. Synthesis of porphyrin-based two-dimensional metal-organic framework nanodisk with small size and few layers. *J. Mater. Chem.* **2018**, *6*, 2828–2833. [[CrossRef](#)]
8. Rocca, J.D.; Lin, W. Nanoscale metal-organic frameworks: Magnetic resonance imaging contrast agents and beyond. *Eur. J. Inorg. Chem.* **2010**, *24*, 3725–3734. [[CrossRef](#)]
9. Qin, L.; Sun, Z.Y.; Cheng, K.; Liu, S.W.; Pang, J.X.; Xia, L.M.; Chen, W.H.; Cheng, Z.; Chen, J.X. Zwitterionic manganese and gadolinium metal-organic frameworks as efficient contrast agents for in vivo magnetic resonance imaging. *ACS Appl. Mater. Interfaces* **2017**, *9*, 41378–41386. [[CrossRef](#)]
10. Wu, M.X.; Yang, Y.W. Metal-organic framework (MOF)-based drug/cargo delivery and cancer therapy. *Adv. Mater.* **2017**, *29*, 1606134. [[CrossRef](#)]
11. Lan, G.; Ni, K.; Veroneau, S.S.; Feng, X.; Nash, G.T.; Luo, T.; Xu, Z.; Lin, W. Titanium-based nanoscale metal-organic framework for type I photodynamic therapy. *J. Am. Chem. Soc.* **2019**, *141*, 4204–4208. [[CrossRef](#)] [[PubMed](#)]
12. Wang, H.; Yu, D.; Fang, J.; Cao, C.; Liu, Z.; Ren, J.; Qu, X. Renal-clearable porphyrinic metal-organic framework nanodots for enhanced photodynamic therapy. *ACS Nano* **2019**, *13*, 9206–9217. [[CrossRef](#)] [[PubMed](#)]

13. Li, H.; Wang, K.; Sun, Y.; Lollar, C.T.; Li, J.; Zhou, H.C. Recent advances in gas storage and separation using metal-organic frameworks. *Mater. Today* **2018**, *21*, 108–121. [[CrossRef](#)]
14. Alezi, D.; Belmabkhout, Y.; Suyetin, M.; Bhatt, P.M.; Weseliński, Ł.J.; Solovyeva, V.; Adil, K.; Spanopoulos, I.; Trikalitis, P.N.; Emwas, A.H.; et al. MOF crystal chemistry paving the way to gas storage needs: Aluminum-based soc-MOF for CH<sub>4</sub>, O<sub>2</sub>, and CO<sub>2</sub> storage. *J. Am. Chem. Soc.* **2015**, *137*, 13308–13318. [[CrossRef](#)] [[PubMed](#)]
15. Fang, Y.; Ma, Y.; Zheng, M.; Yang, P.; Asiri, A.M.; Wang, X. Metal-organic frameworks for solar energy conversion by photoredox catalysis. *Coordin. Chem. Rev.* **2018**, *373*, 83–115. [[CrossRef](#)]
16. Wang, Y.C.; Liu, X.Y.; Wang, X.X.; Cao, M.S. Metal-organic frameworks based photocatalysts: Architecture strategies for efficient solar energy conversion. *Chem. Eng. J.* **2021**, *419*, 129459. [[CrossRef](#)]
17. Eddaoudi, M.; Kim, J.; Rosi, N.; Vodak, D.; Wachter, J.; O’Keeffe, M.; Yaghi, O.M. Systematic design of pore size and functionality in isoreticular MOFs and their application in methane storage. *Science* **2002**, *295*, 469–472. [[CrossRef](#)]
18. Rosi, N.L.; Eckert, J.; Eddaoudi, M.; Vodak, D.T.; Kim, J.; O’Keeffe, M.; Yaghi, O.M. Hydrogen storage in microporous metal-organic frameworks. *Science* **2003**, *300*, 1127–1129. [[CrossRef](#)]
19. Sumida, K.; Rogow, D.L.; Mason, J.A.; McDonald, T.M.; Bloch, E.D.; Herm, Z.R.; Bae, T.H.; Long, J.R. Carbon dioxide capture in metal-organic frameworks. *Chem. Rev.* **2012**, *112*, 724–781. [[CrossRef](#)]
20. Herm, Z.R.; Swisher, J.A.; Smit, B.; Krishna, R.; Long, J.R. Metal-organic frameworks as adsorbents for hydrogen purification and precombustion carbon dioxide capture. *J. Am. Chem. Soc.* **2011**, *133*, 5664–5667. [[CrossRef](#)]
21. McDonald, T.M.; Mason, J.A.; Kong, X.; Bloch, E.D.; Gygi, D.; Dani, A.; Crocellà, V.; Giordanino, F.; Odoh, S.O.; Drisdell, W.S.; et al. Cooperative insertion of CO<sub>2</sub> in diamine-appended metal-organic frameworks. *Nature* **2015**, *519*, 303–308. [[CrossRef](#)] [[PubMed](#)]
22. Taylor-Pashow, K.M.L.; Rocca, J.D.; Xie, Z.; Tran, S.; Lin, W. Postsynthetic modifications of iron-carboxylate nanoscale metal-organic frameworks for imaging and drug delivery. *J. Am. Chem. Soc.* **2009**, *131*, 14261–14263. [[CrossRef](#)] [[PubMed](#)]
23. Horcajada, P.; Serre, C.; Maurin, G.; Ramsahye, N.A.; Balas, F.; Vallet-Regí, M.; Sebban, M.; Taulelle, F.; Férey, G. Flexible porous metal-organic frameworks for a controlled drug delivery. *J. Am. Chem. Soc.* **2008**, *130*, 6774–6780. [[CrossRef](#)]
24. Ni, K.; Lan, G.; Lin, W. Nanoscale metal-organic frameworks generate reactive oxygen species for cancer therapy. *ACS Cent. Sci.* **2020**, *6*, 861–868. [[CrossRef](#)] [[PubMed](#)]
25. Lu, K.; He, C.; Lin, W. A chlorin-based nanoscale metal-organic framework for photodynamic therapy of colon cancers. *J. Am. Chem. Soc.* **2015**, *137*, 7600–7603. [[CrossRef](#)]
26. Park, J.; Jiang, Q.; Feng, D.; Mao, L.; Zhou, H.C. Size-controlled synthesis of porphyrinic metal-organic framework and functionalization for targeted photodynamic therapy. *J. Am. Chem. Soc.* **2016**, *138*, 3518–3525. [[CrossRef](#)]
27. Chen, Q.W.; Liu, X.H.; Fan, J.X.; Peng, S.Y.; Wang, J.W.; Wang, X.N.; Zhang, C.; Liu, C.J.; Zhang, X.Z. Self-mineralized photothermal bacteria hybridizing with mitochondria-targeted metal-organic frameworks for augmenting photothermal tumor therapy. *Adv. Funct. Mater.* **2020**, *30*, 1909806. [[CrossRef](#)]
28. Kreno, L.E.; Leong, K.; Farha, O.K.; Allendorf, M.; Duyne, R.P.V.; Hupp, J.T. Metal-organic framework materials as chemical sensors. *Chem. Rev.* **2012**, *112*, 1105–1125. [[CrossRef](#)]
29. Fang, X.; Zong, B.; Mao, S. Metal-organic framework-based sensors for environmental contaminant sensing. *Nano-Micro Lett.* **2018**, *10*, 64. [[CrossRef](#)]
30. Zhang, Y.; Yuan, S.; Day, G.; Wang, X.; Yang, X.; Zhou, H.C. Luminescent sensors based on metal-organic frameworks. *Coordin. Chem. Rev.* **2018**, *354*, 28–45. [[CrossRef](#)]
31. Luo, J.; Xie, Z.; Lam, J.W.Y.; Cheng, L.; Chen, H.; Qiu, C.; Kwok, H.S.; Zhan, X.; Liu, Y.; Zhu, D.; et al. Aggregation-induced emission of 1-methyl-1,2,3,4,5-pentaphenylsilole. *Chem. Commun.* **2001**, *18*, 1740–1741. [[CrossRef](#)] [[PubMed](#)]
32. Hu, R.; Qin, A.; Tang, B.Z. AIE polymers: Synthesis and applications. *Prog. Polym. Sci.* **2020**, *100*, 101176. [[CrossRef](#)]
33. Ding, D.; Li, K.; Liu, B.; Tang, B.Z. Bioprobes based on AIE fluorogens. *Accounts Chem. Res.* **2013**, *46*, 2441–2453. [[CrossRef](#)] [[PubMed](#)]
34. Shustova, N.B.; McCarthy, B.D.; Dincă, M. Turn-on fluorescence in tetraphenylethylene-based metal-organic frameworks: An alternative to aggregation-induced emission. *J. Am. Chem. Soc.* **2011**, *133*, 20126–20129. [[CrossRef](#)]
35. Wei, Z.; Gu, Z.Y.; Arvapally, R.K.; Chen, Y.P.; Jr, R.N.M.; Ivy, J.F.; Yakovenko, A.A.; Feng, D.; Omary, M.A.; Zhou, H.C. Rigidifying fluorescent linkers by metal-organic framework formation for fluorescence blue shift and quantum yield enhancement. *J. Am. Chem. Soc.* **2014**, *136*, 8269–8276. [[CrossRef](#)]
36. Zhang, Q.; Su, J.; Feng, D.; Wei, Z.; Zou, X.; Zhou, H.C. Piezofluorochromic metal-organic framework: A microscissor lift. *J. Am. Chem. Soc.* **2015**, *137*, 10064–10067. [[CrossRef](#)]
37. Guo, Y.; Feng, X.; Han, T.; Wang, S.; Lin, Z.; Dong, Y.; Wang, B. Tuning the luminescence of metal-organic frameworks for detection of energetic heterocyclic compounds. *J. Am. Chem. Soc.* **2014**, *136*, 15485–15488. [[CrossRef](#)]
38. Zhu, L.; Wong, B.J.C.; Li, Y.; Xin, H.; Liu, B.; Lei, J. Quencher-delocalized emission strategy of AIEgen-based metal-organic framework for profiling of subcellular glutathione. *Chem. Eur. J.* **2019**, *25*, 4665–4669. [[CrossRef](#)]
39. Zhao, Y.; Wang, J.; Zhu, W.; Liu, L.; Pei, R. The modulation effect of charge transfer on photoluminescence in metal-organic frameworks. *Nanoscale* **2021**, *13*, 4505–4511. [[CrossRef](#)]

40. Tsuppayakorn-ae, P.; Bovornratanaraks, T.; Ahuja, R.; Bovornratanaraks, T.; Luo, W. Existence of yttrium allotrope with incommensurate host–guest structure at moderate pressure: First evidence from computational approach. *Comp. Mater. Sci.* **2022**, *213*, 111652. [[CrossRef](#)]
41. Kursunlu, A.N.; Acikbas, Y.; Ozmen, M.; Erdogan, M.; Capan, R. Haloalkanes and aromatic hydrocarbons sensing using Langmuir–Blodgett thin film of pillar[5]arene-biphenylcarboxylic acid. *Colloid. Surface.* **2019**, *565*, 108–117. [[CrossRef](#)]
42. Yuvayapan, S.; Aydogan, A. Counter cation dependent and stimuli responsive supramolecular polymers constructed by calix[4]pyrrole based host–guest interactions. *Eur. J. Org. Chem.* **2019**, *4*, 633–639. [[CrossRef](#)]
43. Zhao, Y.; Wang, J.; Pei, R. Micro-sized ultrathin metal-organic framework sheet. *J. Am. Chem. Soc.* **2020**, *142*, 10331–10336. [[CrossRef](#)] [[PubMed](#)]